JPSE (Journal of Physical Science and Engineering), Vol. 9, No. 2, 2024, Page 121–133.
DOI: 10.17977/um024v9i22024p121

JPSE
(Journal of Physical Science and Engineering)

http://journal2.um.ac.id/index.php/jpse
EISSN: 2541-2485

# Simulation and Impact of Environmental Temperature Changes on Ferrofluid Magnetic Dipoles $Fe_3O_4$-TMAH

**Received**
16 July 2024

**Revised**
20 September 2024

**Accepted for Publication**
5 October 2024

**Published**
31 October 2024

**Aziza Tanzila Meilenia[1], Nadiya Miftachul Chusna[1], Yoyok Adisetio Laksono[1], Hari Wisodo[1] and Sunaryono Sunaryono[1,2*]**

1. Department of Physics, Faculty of Mathematics and Natural Sciences, Universitas Negeri Malang, Jl. Semarang No. 5, Malang 65145, Indonesia.
2. PUI-Centre of Advanced Materials for Renewable Energy (CAMRY), Universitas Negeri Malang, Jl. Semarang No. 5 Malang 65145, Indonesia.

***E-mail:** sunaryono.fmipa@um.ac.id



## Abstract

This research examines the simulation of magnetic dipole interactions in ferrofluids at various environmental temperatures. Ferrofluids have a lot of potential, such as in cooling machines and in the medical field, including magnetic hyperthermia. Apart from focusing on simulations, this research also focuses on ferrofluid experiments. $Fe_3O_4$ nanoparticles were successfully synthesized using the coprecipitation method. The synthesized $Fe_3O_4$ was characterized using XRD which showed that the $Fe_3O_4$ crystal size was around 10.82 nm in the form of a cubic spinel structure. Then ferrofluid was fabricated using TMAH surfactant with variations in $H_2O$ composition. The magnetic properties of the ferrofluid were successfully characterized using the VSM instrument. The results of VSM data analysis show that the saturation magnetization value of ferrofluid with sample codes FTT1, FTT2, and FTT3 is 3.69, 2.61, and 1.97 emu/mL, respectively. The magnetic field of each sample shows a significant increase as the environmental temperature changes from 53 °C to -4 °C. This is because the orientation of the magnetic dipole in the sample is more stable with decreasing environmental temperature, so that the orientation of the sample's magnetic moment becomes more directional. The simulation results show that samples with low ambient temperatures have more regular magnetic dipole moments, thus strengthening the magnetic properties of the ferrofluid. The magnetic dipole moment from the simulation results in a value of $9.50 \times 10^{-3}$ T. The magnetic dipole moment measurement is slightly higher than the experimental results which reached $1.15 \times 10^{-3}$ T. The difference in the magnetic dipole moment between the simulation results and the results experiments can be affected by limitations in the number of particles used in the simulation.

**Keywords:** Simulation, magnetic dipole, ferrofluid.

## 1. Introduction

Ferrofluid is a colloidal suspension of particles dispersed in a certain liquid [1]. The use of ferrofluids is relatively large, for example ferrofluids are used for cooling in hydrodynamics [2], thermoelectric cooling [3], and as a coolant in heat transfer in the hybrid field [4]. Ferrofluids are also used in the medical field, for example magnetic hyperthermia to destroy tumor cells [5]. The various uses of ferrofluids show that ferrofluids have many benefits in everyday life. One of the benefits that is closest to our daily activities is cooling machines [2]. In this case, ferrofluid acts as an increase in the working efficiency of the cooling fan. Apart from that, the use of ferrofluids in the research of S. Wiriyasart et al. can overcome space limitations in cooling machines [3]. Based on research by M. Bezaatpour and M. Goharkhah, the working efficiency of the cooling fan reaches 35% after using ferrofluid [2]. However, the performance of ferrofluid in cooling machines is also influenced by environmental temperature. This is caused by the decrease in ferrofluid viscosity at high temperatures [4, 6]. This decrease in viscosity will have an impact on the magnetic field of the ferrofluid. However, the presence of a ferrofluid magnetic field will indirectly affect the performance of the ferrofluid in the cooling machine.

There is quite a lot of research on ferrofluid simulation, such as research by H. Abbasov on modeling anisotropic thermal conductivity of ferrofluids [7], by S. M. Mousavi on modeling and simulating the flow and heat transfer of ferrofluids under the magnetic field of neodymium block magnets [8], and research by R. M. Oliveira and J. A. Miranda on the simulation of completely nonlinear ferrofluid patterns in a radial magnetic field [9]. Although there has been a lot of research on ferrofluid simulation, there is still little ferrofluid research on dipole simulation at various temperatures. However, it is rarely reported about ferrofluid magnetic fields and magnetic dipole conditions in certain conditions, therefore this research will examine the use of ferrofluids under temperature variations.

In magnetic dipole simulations, a mathematical model is needed to determine the orientation of the magnetic dipole relative to temperature. However, we can know the interaction of electromagnetic forces in ferrofluids. In this research, Matplotlib is used as software to understand the interactions between ferrofluid magnetic dipoles in temperature variations. Matplotlib is a 2D graphics package used for Python [10]. Matplotlib is widely used to create static, animated and interactive visualizations in Python [11]. There are many graph functions for creating graphs, diagrams and other visualizations [12]. To visualize data, Matplotlib usually uses NumPy as a reference [13]. Matplotlib, which uses a mathematical model with Langevin parameters, will provide an illustration of the influence of heat energy on particle energy in a magnetic field [7]. This research allows modeling of particle interactions in ferrofluids under various temperature conditions, which is difficult to achieve through purely physical experiments. This simulation will analyze the dipole response in ferrofluids to changes in temperature which has not been widely studied.

Experimentally, $Fe_3O_4$ was synthesized using the coprecipitation method. Characterization using XRD was carried out on the $Fe_3O_4$ powder sample to determine the crystal structure of the sample. Then $Fe_3O_4$ paste was fabricated with TMAH as a surfactant in the ferrofluid and $H_2O$ as a dispersing medium in the ferrofluid. Characterization of the magnetic properties of $Fe_3O_4$-TMAH ferrofluid using VSM. To be able to apply it to changes in environmental temperature, it is necessary to study ferrofluid magnetic dipole under various conditions. In this research, temperature variations were applied at 53, 25, 14, and -4 °C

## 2. Method

### *2.1. Synthesis of $Fe_3O_4$-TMAH Ferrofluid*

In this research, the raw material for synthesizing $Fe_3O_4$ nanoparticles is iron sand and the method used is coprecipitation. The first step in $Fe_3O_4$ synthesis is the separation of iron sand using a permanent magnet. After obtaining pure iron sand, the next step is to react the pure iron sand with hydrogen chloride (12.063 M, Merck) to produce a solution of $FeCl_3$ and $FeCl_2$. Then the $FeCl_3$

and $FeCl_2$ solutions were titrated using ammonium hydroxide solution (6.5 M, Merck) until a precipitate was formed and a precipitate was produced. The precipitate was then washed using water until it reached PH = 7 and $Fe_3O_4$ nanoparticles were obtained. Then the $Fe_3O_4$-TMAH ferrofluid fabrication was synthesized using $Fe_3O_4$ nanoparticles and TMAH as surfactant. The process involves precipitation of $Fe_3O_4$ with a neutral pH, mixed with 0.5 ml of TMAH while stirring for 10 minutes. Next, $H_2O$ with a certain composition (shown in Table 1.) is added to the mixture and stirred until homogeneity is achieved.

**Table 1.** $H_2O$ composition and sample nomenclature.

| $H_2O$ Composition (ml) | Sample Names |
|---|---|
| 0.1 | FTT 1 |
| 0.3 | FTT 2 |
| 0.5 | FTT 3 |

### *2.2. Characterization*

Crystal structure characterization was carried out using X-ray diffraction (XRD) PANalytical Brand, Type:X'Pert PRO using Cu–K$\alpha$ at $2\theta$ = 20–80º. Magnetic properties were obtained from the Oxford VSM 1.2H characterization tool with an external magnetic field of 1T. Magnetic field characterization was carried out using a set of tools consisting of a gauss meter, permanent magnet, thermocouple, static, and containers with volumes of 1, 2, 3 and 4 cm$^3$. The temperatures used were 53, 25, 14, and -4 ºC. The process of collecting magnetic field data begins by conditioning the container and various ferrofluid samples at the specified temperature for 10 minutes. To validate accuracy, the temperature was measured using a thermocouple. When the temperature has stabilized for a specified time, the magnetic field is measured using a gauss meter and a permanent magnet. Calculating the magnetic field in a set of permanent magnet devices and containers without varying ferrofluid samples. Then a variety of ferrofluid samples are added to the container. The result of magnetic field characterization is the difference from data collection.

### *2.3. Magnetic Dipole Simulation*

The magnetic dipole simulation in this research uses Matplotlib software. First, the references used are imported from NumPy and Matplotlib, for numerical operations and for data visualization, respectively. The temperature and magnetic field were adjusted according to experimental experiments to understand the response of the magnetic dipole to changes in temperature. The simulation results will be compared with the experimental results. In experimental calculations, this research uses the molecular field formula or Weiss field in equation (1).

$$\mu = \frac{M}{H} \tag{1}$$

where, $\mu$ is the magnitude of the magnetic dipole moment, $M$ is the magnetization value obtained from the test results using VSM, and $H$ is the external magnetic field obtained from the results of magnetic field measurements. Then simulated using equation (2).

$$\mu = \frac{\alpha k_B T}{\mu_0 B} \tag{2}$$

where $B$ represents the magnetic field strength, $k_B$ is the Boltzmann constant, $T$ is the temperature of the ferrofluid, and $\mu_0$ is the vacuum permeability.

## 3. Results and Discussion

### *3.1. XRD Pattern of $Fe_3O_4$ Nanoparticles*

The $Fe_3O_4$ nanoparticles produced in this research were characterized using XRD and produced the XRD pattern presented in Figure 1. Figure 1 is also equipped with a red line which is the result of analysis carried out by matching the ICSD 30860 model data with the $Fe_3O_4$ XRD pattern using the Rietveld method with Rietica software. The analysis results show that the highest peak was detected at $2\theta = 35.63^{\circ}$ with the Bragg field (311). These results are similar to L.L. Adebayo, et al (2020) [14]. Other sample peaks were detected at $2\theta$ around (220), (311), (400), (422), (511), and (440) [15]. Based on this analysis, information was also obtained that the $Fe_3O_4$ sample in this study had a cubic spinel structure with the FD3M space group [16]. The cubic spinel structure has $\alpha = \beta = \gamma = 90^{\circ}$ and lattice parameters a, b, and c of about 8.363 Å. The samples produced in this research are nanoscale particles with a crystal size of around 10.82 nm. This result has a relatively similar value to previous research by Tom, et al, namely around 10.3 nm [17]. The XRD pattern analysis in Figure 1 has a high degree of suitability as indicated by *Rp, Rwp,* and *GOF* values of 20.32, 28.20, and 1.20, respectively.

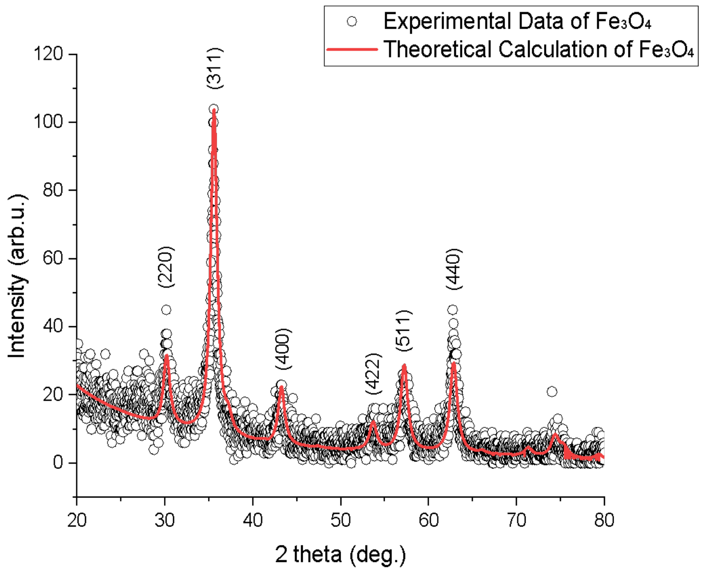


**Figure 1.** XRD pattern of $Fe_3O_4$ nanoparticles.

### *3.2. Magnetic Properties of $Fe_3O_4$-TMAH Ferrofluid*

The magnetic properties of $Fe_3O_4$-TMAH ferrofluid were characterized using a VSM instrument. The $Fe_3O_4$-TMAH ferrofluid hysteresis loop of the VSM instrument is shown in Figure 2. Figures 2(a), 2(b), and 2(c) are the hysteresis loops of FTT 1, FTT 2, and FTT 3 with the respective theoretical lines with Langevin's formula. Langevin's formula according to equation (3).

$$M = M_s\left[\coth\left(\frac{\mu H}{k_B T}\right) - \frac{k_B T}{\mu H}\right] + \chi H + M_r \tag{3}$$

where $M$ is the total magnetic moment (emu/ml), $H$ is the external magnetic field ($T$), $\mu$, magnetic moment (emu), $k_B$ is the Stefan Boltzman constant value ($1.38 \times 10^{-23}$ J/K), $Ms$ is saturation magnetization (emu/ml) [18], $Mr$ respectively and remanent magnetization (emu/ml) [19], $T$ is the temperature ($K$) at the time of characterization using VSM, and $\chi$ is the susceptibility of the sample [20].

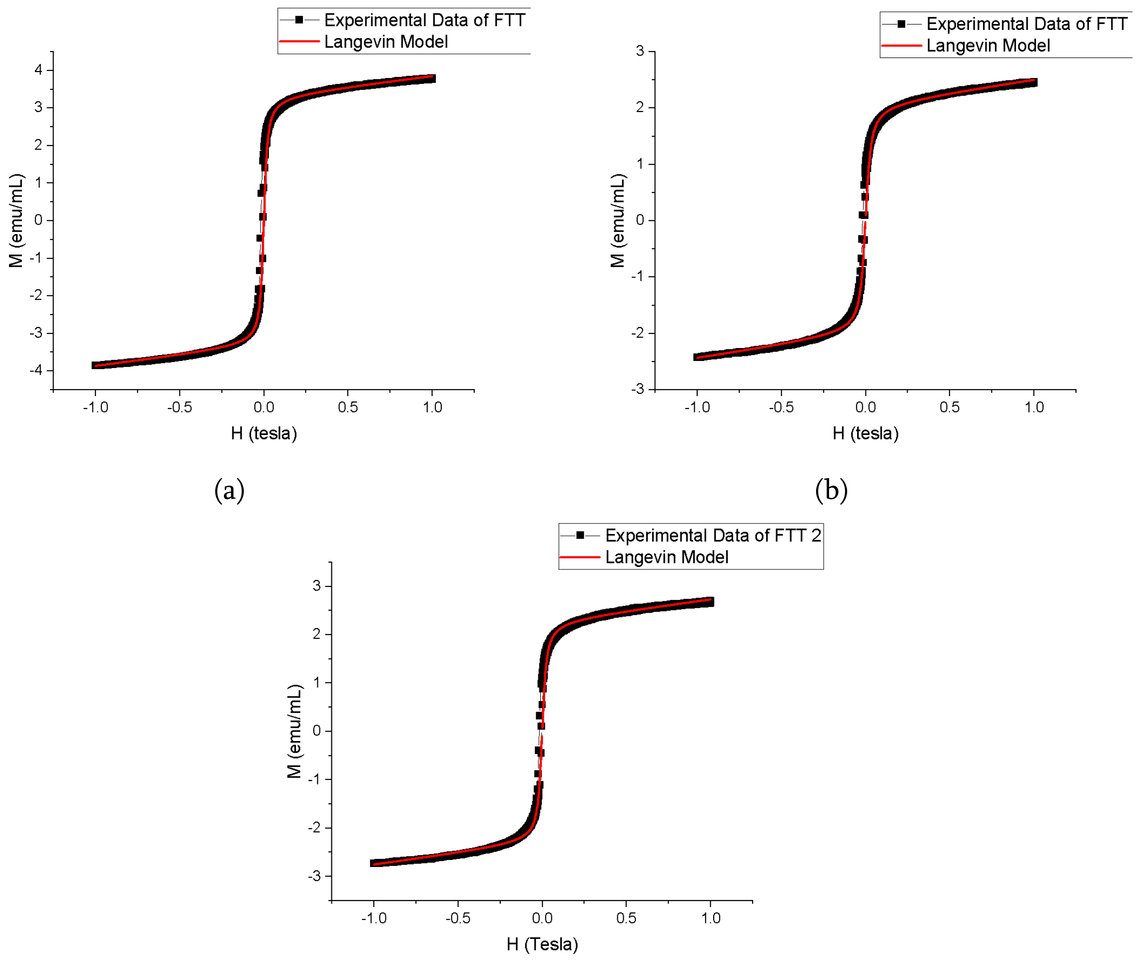


(a) (b)

(c)

**Figure 2.** Hysteresis loops (a) FTT 1, (b) FTT 2, and (c) FTT 3 are marked in black, while the Langevin model is represented in red.

Information on the results of Langevin formula calculations is shown in Table 2. Based on Table 2, it can be seen that the increasing $H_2O$ content in the ferrofluid causes the saturation magnetization value to decrease. In this case, water molecules can form a molecular layer around the nanoparticles which can create a physical barrier between the nanoparticles [21]. This situation will allow the magnetic domain to become smaller in size until it becomes a single domain. This allows the domain to become saturated at low magnetization. The coercivity ($Hc$) field value of the sample shown is close to zero. This value is supported by the S-shaped shape of the hysteresis loop. This shape shows that the $Fe_3O_4$-TMAH ferrofluid has superparamagnetic properties [22]. These results are in line with research by L.S. Ganapathe et al., after the dispersion medium is reduced, the saturation magnetization value increases [23].

**Table 2.** Results of loop hysteresis analysis using the Langevin model.

| Sample Name | $M_s$ (emu/ml) | $M_r$ (emu/ml) | $H_c$ (Tesla) | $\chi$ |
|---|---|---|---|---|
| FTT 1 | 3.692 | 0.011 | 0.012 | 0.552 |
| FTT 2 | 2.612 | 0.013 | 0.013 | 0.459 |
| FTT 3 | 1.968 | 0.020 | 0.008 | 0.312 |

### 3.3. *$Fe_3O_4$-TMAH Ferrofluid Magnetic Field*

The magnetic field value of the $Fe_3O_4$-TMAH ferrofluid was recorded with a gauss meter. The characterization process has been documented in Figure 3. Figure 3(a) is documentation of the measurement of the magnetic field value of $Fe_3O_4$-TMAH ferrofluid using a Gauss meter. Figures 3(b), 3(c), and 3(d) are the process of measuring the magnetic field values of $Fe_3O_4$-TMAH ferrofluid at temperatures of 53, 25, 14, and -4°C respectively and sample volumes of around 1, 2, 3, and 4 $cm^3$. Setting for measuring the magnetic field value of the $Fe_3O_4$-TMAH ferrofluid using a Gauss meter at a normal temperature of 25°C where the observations use a thermometer.

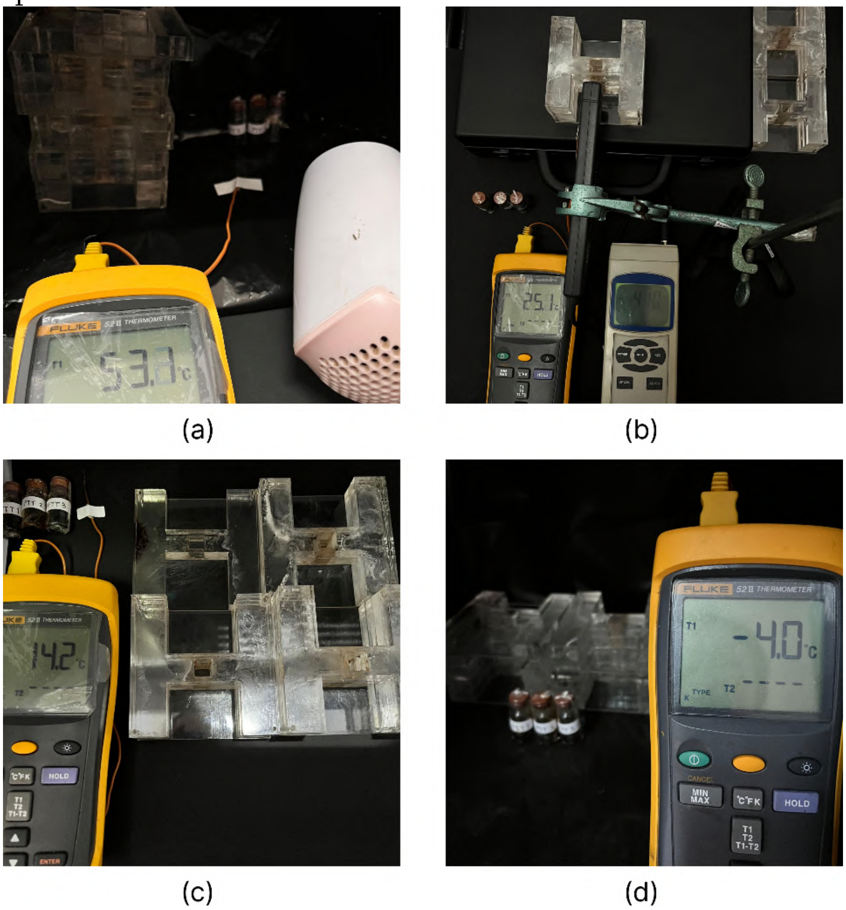


**Figure 3.** Instrument for measuring the magnetic field value of $Fe_3O_4$-TMAH ferrofluid with temperature settings monitored using a thermometer at (a) 53°C, (b) 14°C, and (d) -4°C. Setup for measuring the magnetic field value of $Fe_3O_4$-TMAH ferrofluid using a Gauss meter at a normal temperature of 25°C which is monitored using a thermometer.

Measurement of the magnetic field value of the $Fe_3O_4$-TMAH ferrofluid based on Figure 3 produces magnetic field value data at three different temperature conditions. These results are shown in Table 3. Measurements of magnetic field values were carried out with different volumes of the samples tested to ensure data validation. The graph of the magnetic field value against temperature is shown in Figure 4. Based on Figure 4, the volume of the sample tested is directly proportional to the magnetic field value at the same temperature. Furthermore, the temperature is inversely proportional to the average magnetic field value of the difference in sample volume. The magnetic field increases at low temperatures because at low temperatures the motion of particles becomes more restricted. However, the magnetic moment of the sample becomes more directed. This has an impact on increasing the magnetic field value. Previous studies by Jain et al. (2018) when $Fe_3O_4$ ferrofluid at low temperature conditions showed an increase in the saturation magnetic value, this confirmed that the magnetic field would increase at low temperature conditions [24]. A study by A. A. Ibiyemi et al. (2021) shows that the magnetic field value increases with low temperatures [25]. The study by W. Li et al. (2023) found that the magnetic field decreased due to the viscosity of the ferrofluid which decreased with increasing temperature [26].

**Table 3.** Magnetic field values based on different temperature conditions during measurement.

| Volume ($cm^3$) | Temperature (°C) | Magnetic Field (mT) | | | | | |
|---|---|---|---|---|---|---|---|
| | | FTT 1 | Average of FTT 1 | FTT 2 | Average of FTT 2 | FTT 3 | Average of FTT 3 |
| 1 | 53 | 0.9 | 1.38 | 0.6 | 0.9 | 0.3 | 0.60 |
| 2 | | 1.1 | | 0.8 | | 0.6 | |
| 3 | | 1.7 | | 1.0 | | 0.7 | |
| 4 | | 1.8 | | 1.2 | | 0.8 | |
| 1 | 25 | 2.9 | 3.05 | 1.8 | 2.72 | 2.5 | 2.68 |
| 2 | | 3.1 | | 4.1 | | 2.6 | |
| 3 | | 3.1 | | 2.4 | | 2.3 | |
| 4 | | 3.1 | | 2.6 | | 3.3 | |
| 1 | 14 | 3.1 | 3.40 | 2.4 | 2.72 | 2.3 | 2.55 |
| 2 | | 3.5 | | 2.7 | | 2.4 | |
| 3 | | 3.4 | | 2.6 | | 2.6 | |
| 4 | | 3.6 | | 3.2 | | 2.9 | |
| 1 | -4 | 3.3 | 3.55 | 3.2 | 3.52 | 2.7 | 3.05 |
| 2 | | 3.4 | | 3.3 | | 2.8 | |
| 3 | | 3.6 | | 3.7 | | 3.2 | |
| 4 | | 3.9 | | 3.9 | | 3.5 | |

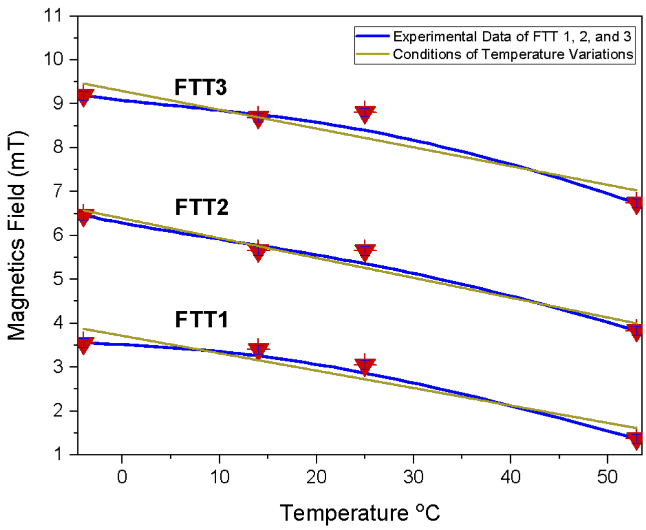


**Figure 4.** Magnetic field values and temperature variations. Experimental data for FTT 1, FTT 2, and FTT 3 are represented by blue lines. Temperature variation conditions are depicted with green lines.

### 3.4. *Magnetic Dipole Simulation of $Fe_3O_4$-TMAH Ferrofluid*

Figures 5(a)-(d) are simulations of the interaction between magnetic dipoles of FTT 1 sample respectively at temperatures of 53, 25, 14, and -4ºC. Figures 5(e)-(h) are the results of simulations of the interaction between magnetic dipoles of the FTT 2 sample at temperatures of 53, 25, 14, and -4ºC, respectively. Meanwhile, Figures 5(i)-(l) represent the interactions between magnetic dipoles of FTT 3 samples respectively at temperatures of 53, 25, 14, and -4ºC. Based on Figure 5, samples FTT 1, FTT 2, and FTT 3 at a temperature of 53ºC (Figure 5(a), (e) and (i)) show that the magnetic dipole in the ferrofluid is more disordered than at temperatures of 14 and -4ºC . While samples FTT 1, FTT 2, and FTT 3 at 25ºC (Figure 5(b), (f) and (i)) the ferrofluid magnetic dipole is relatively ordered but not completely organized as at lower temperatures such as at 14 and - 4ºC. This occurs due to the interaction of electromagnetic motion between $Fe_3O_4$ particles in the ferrofluid due to changes in temperature. As temperature increases, particle interactions become more random. Meanwhile, when the temperature is lower, the interactions of $Fe_3O_4$ particles become more organized.

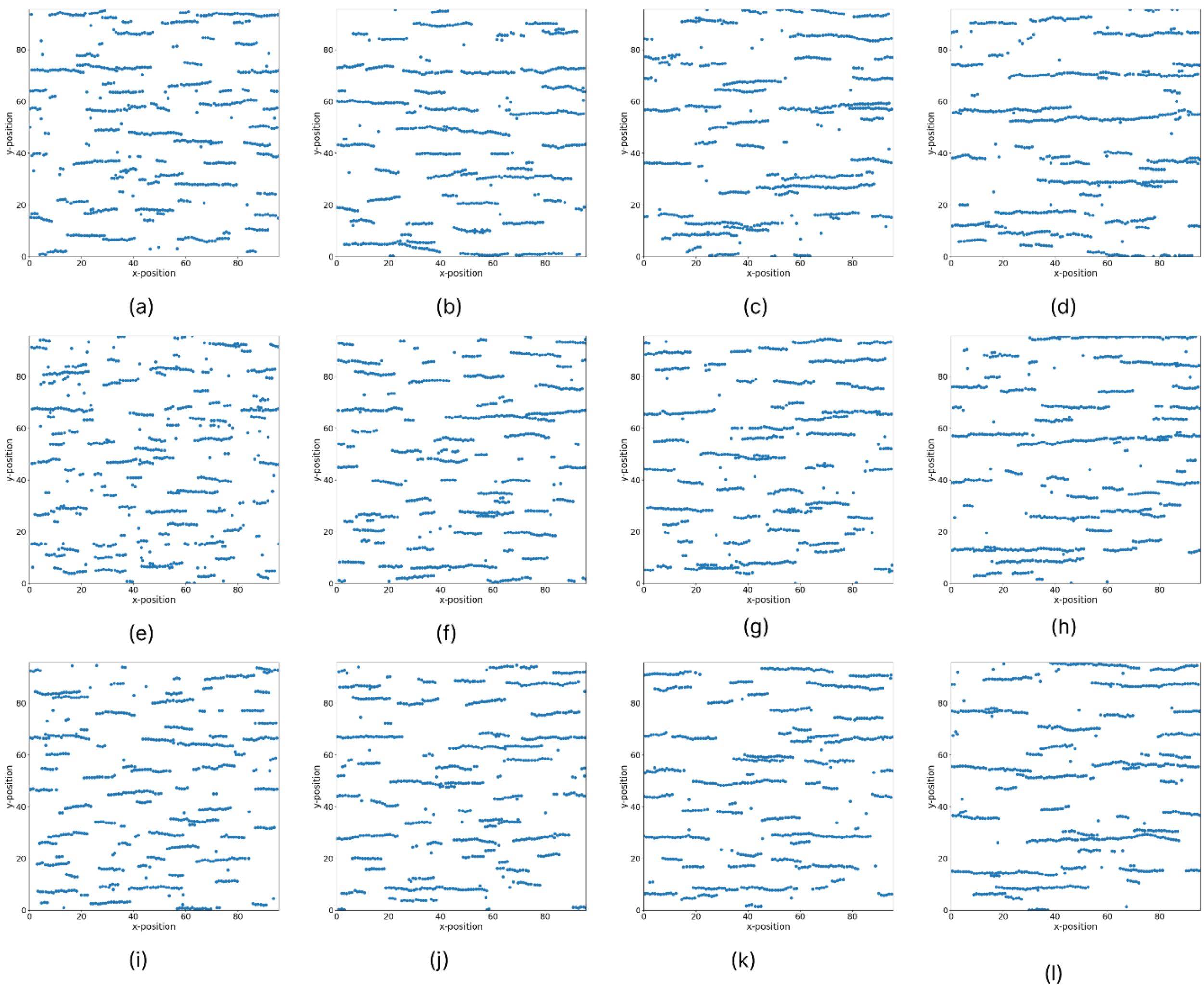


**Figure 5.** Simulation of interaction between magnetic dipoles (a) FTT1 at 53°C (b) FTT 1 at 25°C (c) FTT 1 at 14°C (d) FTT 1 at -4°C (e) FTT 2 at 53°C (f) FTT 2 at 25°C (g) FTT 2 at 14°C (h) FTT 2 at -4°C (i) FTT 3 at 53°C (j) FTT 3 at 25°C (k) FTT 3 at 14°C (l) FTT 3 at -4°C

Simulation of the interaction between the three magnetic dipole samples at a temperature of 14 ºC (Figure 5(c) sample FTT 1, (g) sample FTT 2, and (k) sample FTT3) shows that the particles in the ferrofluid appear more orderly and organized than at this temperature 53 ºC. A decrease in temperature reduces the random movement of particles, so that particles are more likely to move orderly and close to each other. This causes the particles in the ferrofluid to become structured. Meanwhile, the simulation of the interaction between the magnetic dipoles of the three samples at a temperature of -4 ºC is shown in Figure 5(d), FTT sample 1, (h) FTT sample 2, and (l) FTT sample 3 show more regular and strong behavior. Very low temperatures reduce the movement of particles, so that the particles are arranged in an organized manner. The simulation results of this ferrofluid magnetic dipole show that when the temperature decreases, the magnetic dipole moment tends to increase [27]. This means that the particles in the ferrofluid are more ordered at lower temperatures. Particles respond to changes in thermal energy, whereas at low temperatures, thermal energy is more limited, allowing particles to be better organized [28].

Figure 5 is the result of a computer simulation illustrating the behavior of particles in a ferrofluid in response to variations in temperature and magnetic field. It is clearly visible in Figure 5 that there are particles that are clustered and particles that move freely without crowding. In Figure 6, the simulation shows that the blue color is clustered particles (an organized structure of a larger number of particles) and the red color is particles that move freely without crowding. The blue color in the image is used to mark regions where the magnetic dipoles of the ferrofluid particles are better organized or have greater strength. This simulation uses input data based on particle size, temperature and magnetic field parameters obtained from the characterization results carried out in this research.

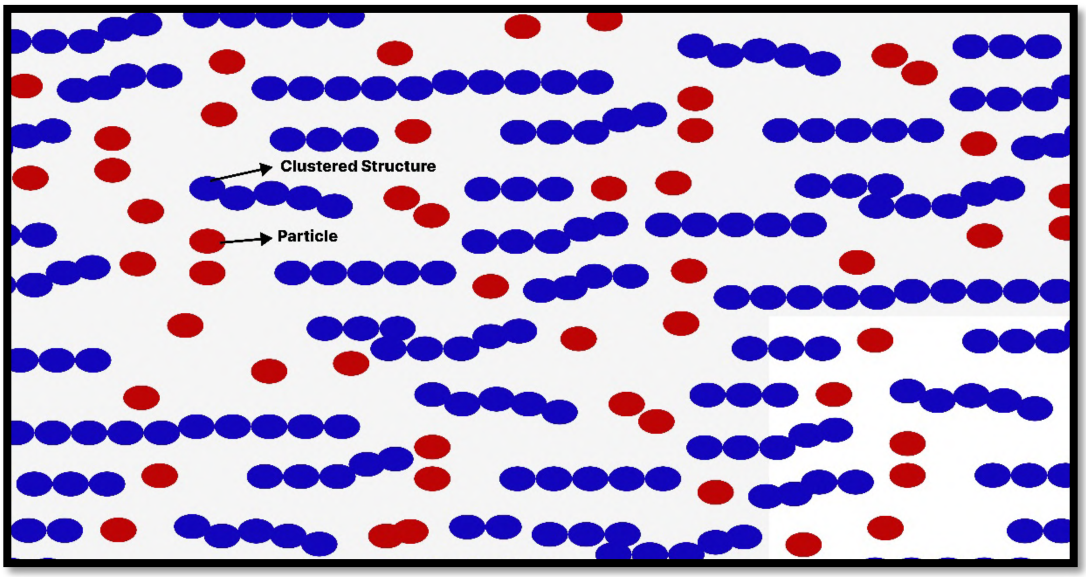


**Figure 6.** The difference between clustered (blue chains) and particle (red circles) structures.

This research shows that ferrofluids have a unique response to magnetic fields, namely particle direction and particle distribution. Particles in a ferrofluid system have a magnetic moment that produces a force between two magnetic dipole moments. Therefore, the potential energy of the dipole-dipole interaction is shown in equation (4).

$$U_{DD} = \frac{\mu_0}{4\pi}\left(\frac{\vec{\mu_1}\cdot\vec{\mu_2}}{r^3} - 3\frac{\left(\vec{\mu_1}\cdot\hat{r}\right)\left(\vec{\mu_2}\cdot\hat{r}\right)}{r^3}\right) \tag{4}$$

$U_{DD}$ is the interaction potential between two particles, $\hat{r}$ is the unit vector, $\vec{\mu_1}$ and $\vec{\mu_2}$ represents the vectors of particles 1 and 2, and $r$ represents the distance between the particles. The first term

$\left(\frac{\overrightarrow{\mu_1}\cdot\overrightarrow{\mu_2}}{r^3}\right)$ indicates an attraction-attraction interaction, while the second term $\left(3\frac{\left(\overrightarrow{\mu_1}\cdot\hat{r}\right)\left(\overrightarrow{\mu_2}\cdot\hat{r}\right)}{r^3}\right)$ represents a repulsion-repulsion interaction. To prevent overlapping particle interactions, the potential formula $u_{sr}^{WCA}$ shown in equation (5) is used.

$$u_{sr}^{WCA} = 4\varepsilon_{12}\left[\left(\frac{\sigma}{r_{12}}\right)^{12} - \left(\frac{\sigma}{r_{12}}\right)^{6}\right] + \varepsilon_{12} \tag{5}$$

If in the case where $r_{12} < r_{cut}$, then equation (5) becomes $u_{sr}^{WCA} = 0$. Here $u_{sr}^{WCA}$ is the central potential with the Weeks-Chandler-Andersen potential (WCA), WCA is used in molecular dynamics to model interactions between particles in systems. $\varepsilon_{12}$ represents the potential energy dependent on particles 1 and 2, while $\sigma$ represents the diameter of the particles, $r_{12}$ represents the radius between two particles, $r_{cut}$ and represents the boundary radius, where $r_{cut} = r_{\min} = 2^{\frac{1}{6}}\cdot\sigma$. To prove it, it is considered $r = 2^{\frac{1}{6}}\cdot\sigma$, shown in equation (6).

$$\begin{aligned} u_{sr}^{WCA} &= 4\varepsilon_{12}\left[\left(\frac{\sigma}{2^{\frac{1}{6}}\cdot\sigma}\right)^{12} - \left(\frac{\sigma}{2^{\frac{1}{6}}\cdot\sigma}\right)^{6}\right] + \varepsilon_{12} \\ &= 4\varepsilon_{12}\left[\frac{1^{12}}{2^2} - \frac{1^6}{2^1}\right] + \varepsilon_{12} \\ &= 4\varepsilon_{12}\left[\frac{1}{4} - \frac{1}{2}\right] + \varepsilon_{12} \\ &= 4\varepsilon_{12}\left[-\frac{1}{4}\right] + \varepsilon_{12} \\ &= -\varepsilon_{12} + \varepsilon_{12} \\ &= 0 \end{aligned} \tag{6}$$

thus, the stated total potential can be expressed as the sum of the total dipole-dipole potential and the WCA potential shown in equation (7).

$$u_{total} = u_{sr}^{WCA} + u_{DD} \tag{7}$$

in a ferrofluid system, there are three important parameters. Firstly, the area of the two-dimensional fraction. Then the second is the dipolar interaction parameter expressed as in equation (8).

$$\lambda = \frac{\tilde{u}_{DD}}{u_T} \tag{8}$$

Note $\lambda$ is a dipole interaction parameter, $\tilde{u}_{DD}$ represents the absolute value of the dipole-dipole interaction energy, and $u_T$ represents the thermal energy. To simplify calculations, this research takes the attractive interaction at the dipole-dipole potential and uses thermal potential energy as in equation (9).

$$U_T = k_B T \tag{9}$$

So that,

$$\lambda = \frac{\mu_0}{4\pi}\frac{\mu_1\mu_2}{r^3}\frac{1}{k_B T}$$
$$= \frac{\mu_0}{4\pi}\frac{\mu_2}{k_B T r^3} \tag{10}$$

The third parameter is the external magnetic field using the Langevin parameter $\alpha$ which is the ratio of temperature to mass, so the magnetic moment is expressed as in equation (2). Calculation of the dipole moment from experimental results uses the molecular field formula or Weiss field as in equation (1). This means that the greater the value of the dipole moment, the greater the resulting magnetization [29].

These simulation results show differences compared to experimental results. The magnetic dipole moment simulation produces a value of $9.5 \times 10^{-3}$ T, while the experimental results reach $1.146 \times 10^{-3}$ T. This is because the number of particles in the simulation using Matplotlib is limited to only 700 particles and cannot accurately describe the complexity of interactions between particles in ferrofluid. So Matplotlib is not the most efficient reference for producing complex visualizations with large-scale particle numbers [30]. A previous review from A. Lavanya et al also stated that this happened because the visualization results in the simulation were limited [30]. Experimental calculations use the molecular field formula or Weiss field with magnetization values from the VSM test and external magnetic fields measured from the results of magnetic field measurements. This means that the greater the dipole moment, the greater the resulting magnetization, according to equation (3).

## 4. Conclusion

Ferrofluid $Fe_3O_4$-TMAH has been successfully synthesized and produces a crystal structure of $Fe_3O_4$ nanoparticles measuring around 10.3 nm. The crystal structure of the sample was detected as a cubic spinel structure. The magnetic properties of $Fe_3O_4$-TMAH ferrofluid were characterized using VSM and the resulting hysteresis loop. The hysteresis loop shape shows that the sample has superparamagnetic material with sample saturation magnetization values of 3.692, 2.61, and 1.98 emu/ml for $H_2O$ content in ferrofluid of 0.1, 0.3, and 0.5 ml, respectively. Based on these results, adding $H_2O$ content can reduce the magnetization saturation value. The magnetic field value of the $Fe_3O_4$-TMAH ferrofluid was measured with a gauss meter. This characterization results in the magnetic field value of the sample increasing as the temperature decreases. The simulation results show that when the temperature is lowered, the magnetic dipole moment tends to increase. This means that the particles in the ferrofluid are more ordered at lower temperatures. However, there is a difference between the simulation and experimental results, namely the value of the magnetic dipole moment in the simulation results is lower. The magnetic dipole moment simulation produces a value of $9.5 \times 10^{-3}$ T, while the experimental results reach $1.146 \times 10^{-3}$ T. The limited number of particles in the simulation can influence these results. So Matplotlib is not very accurate in describing the complexity of interactions between particles in ferrofluids. This study also proves the molecular field formula or Weiss field that the greater the dipole moment, the greater the resulting magnetization.

## Acknowledgment

This research was fully funded by the Internal Funds of the State University of Malang in 2024, Master's Thesis Research Scheme (PTM) contract 4.4.660/UN32.14.1/LT/2024 on behalf of SN.

## References

[1] J. Philip, "Magnetic nanofluids (Ferrofluids): Recent advances, applications, challenges, and future directions," *Adv. Colloid Interface Sci.*, vol. 311, p. 102810, Jan. 2023, doi: 10.1016/j.cis.2022.102810.

[2] M. Bezaatpour and M. Goharkhah, "Effect of Magnetic Field on the Hydrodynamic and Heat Transfer of Magnetite Ferrofluid Flow in a Porous Fin Heat Sink," *J. Magn. Magn. Mater.*, vol. 476, pp. 506–515, 2019.

[3] S. Wiriyasart, P. Suksusron, C. Hommalee, A. Siricharoenpanich, and P. Naphon, "Heat Transfer Enhancement of Thermoelectric Cooling Module with Nanofluid and Ferrofluid as Base Fluids," *Case Stud. Therm. Eng.*, vol. 24, p. 100877, 2021.

[4] S. O. Giwa, M. Sharifpur, and J. P. Meyer, "Effects of Uniform Magnetic Induction on Heat Transfer Performance of Aqueous Hybrid Ferrofluid in a Rectangular Cavity," *Appl. Therm. Eng.*, vol. 170, p. 115004, Apr. 2020.

[5] M. S. Darwish *et al.*, "The Heating Efficiency and Imaging Performance of Magnesium Iron Oxide tetramethyl Ammonium Hydroxide Nanoparticles for Biomedical Applications," *Nanomaterials*, vol. 11, no. 5, p. 1096, 2021.

[6] Á. Sanz-Felipe and J. C. Martín, "Analysis of temperature dependence in ferrofluid optical transmission dynamics after magnetic field commutation," *J. Magn. Magn. Mater.*, vol. 529, p. 167836, Jul. 2021.

[7] H. Abbasov, "Modeling of anisotropic thermal conductivity of ferrofluids," *J. Dispers. Sci. Technol.*, vol. 41, no. 7, pp. 1030–1036, Jun. 2020, doi: 10.1080/01932691.2019.1614040.

[8] S. M. Mousavi, A. A. R. Darzi, and M. Li, "Modelling and Simulation of Flow and Heat Transfer of Ferrofluid under Magnetic Field of Neodymium Block Magnet," *Appl. Math. Model.*, vol. 103, pp. 238–260, Mar. 2022, doi: 10.1016/j.apm.2021.10.019.

[9] R. M. Oliveira and J. A. Miranda, "Fully nonlinear simulations of ferrofluid patterns in a radial magnetic field," *Phys. Rev. Fluids*, vol. 5, no. 12, p. 124003, Dec. 2020, doi: 10.1103/PhysRevFluids.5.124003.

[10] D. Nedelcu and T. Latinovic, "PyChart – A Python module for analysis and visual view of 2D/3D Charts," *J. Phys. Conf. Ser.*, vol. 1781, no. 1, p. 012044, Feb. 2021, doi: 10.1088/1742-6596/1781/1/012044.

[11] L. Addepalli *et al.*, "Assessing the Performance of Python Data Visualization Libraries: A Review," *Int. J. Comput. Eng. Res. Trends*, vol. 10, pp. 28–39, Jan. 2023, doi: 10.22362/ijcert/2023/v10/i01/v10i0104.

[12] S. Cao, Y. Zeng, S. Yang, and S. Cao, "Research on Python Data Visualization Technology," *J. Phys. Conf. Ser.*, vol. 1757, no. 1, p. 012122, Jan. 2021, doi: 10.1088/1742-6596/1757/1/012122.

[13] C. R. Harris *et al.*, "Array programming with NumPy," *Nature*, vol. 585, no. 7825, pp. 357–362, Sep. 2020, doi: 10.1038/s41586-020-2649-2.

[14] L. L. Adebayo *et al.*, "Recent advances in the development of $Fe_3O_4$-based microwave absorbing materials," *Ceram. Int.*, vol. 46, no. 2, pp. 1249–1268, Feb. 2020, doi: 10.1016/j.ceramint.2019.09.209.

[15] A. T. Semeano *et al.*, "Effects of Magnetite Nanoparticles and Static Magnetic Field on Neural Differentiation of Pluripotent Stem Cells," *Stem Cell Rev. Rep.*, vol. 18, no. 4, pp. 1337–1354, Apr. 2022, doi: 10.1007/s12015-022-10332-0.

[16] S. Kumar, M. Kumar, and A. Singh, "Synthesis and characterization of iron oxide nanoparticles: a brief review," *Contemp. Phys.*, vol. 62, no. 3, pp. 144–164, Jul. 2021, doi: 10.1080/00107514.2022.2080910.

[17] G. Tom, S. Philip, R. Isaac, P. K. Praseetha, S. G. Jiji, and V. V. Asha, "Preparation of an efficient and safe polymeric-magnetic nanoparticle delivery system for sorafenib in hepatocellular carcinoma," *Life Sci.*, vol. 206, pp. 10–21, Aug. 2018.

[18] S. Sunaryono *et al.*, "The effect of Fe3O4 concentration to photocatalytic activity of $Fe_3O_4$@$TiO_2$-PVP core-shell nanocomposite," *J. Phys. Conf. Ser.*, vol. 1595, no. 1, p. 012003, Jul. 2020, doi: 10.1088/1742-6596/1595/1/012003.

[19] G. Asab, E. A. Zereffa, and T. Abdo Seghne, "Synthesis of Silica-Coated $Fe_3O_4$ Nanoparticles by Microemulsion Method: Characterization and Evaluation of Antimicrobial Activity," *Int. J. Biomater.*, vol. 2020, p. e4783612, Mar. 2020.

[20] K. Wu, D. Su, J. Liu, R. Saha, and J.-P. Wang, "Magnetic Nanoparticles in Nanomedicine".

[21] A. Zen *et al.*, "Long-Range Ionic and Short-Range Hydration Effects Govern Strongly Anisotropic Clay Nanoparticle Interactions," *J. Phys. Chem. C*, vol. 126, no. 18, pp. 8143–8151, May 2022, doi: 10.1021/acs.jpcc.2c01306.

[22] P. N. Oliveira *et al.*, "Magnetite nanoparticles with controlled sizes via thermal degradation of optimized PVA/Fe (III) complexes," *J. Magn. Magn. Mater.*, vol. 460, pp. 381–390, 2018.

[23] L. S. Ganapathe, M. A. Mohamed, R. Mohamad Yunus, and D. D. Berhanuddin, "Magnetite ($Fe_3O_4$) Nanoparticles in Biomedical Application: From Synthesis to Surface Functionalisation," *Magnetochemistry*, vol. 6, no. 4, p. 68, Dec. 2020.

[24] R. Jain, V. Luthra, and S. Gokhale, "Probing influence of rare earth ions on structural, magnetic and optical properties of magnetite nanoparticles," *J. Magn. Magn. Mater.*, vol. 456, pp. 179–185, Jun. 2018.

[25] A. A. Ibiyemi, G. T. Yusuf, and A. Olusola, "Influence of temperature and magnetic field on rheological behavior of ultra-sonicated and oleic acid coated cobalt ferrite ferrofluid," *Phys. Scr.*, vol. 96, no. 12, p. 125842, Dec. 2021, doi: 10.1088/1402-4896/ac2ecb.

[26] W. (李望旭) Li *et al.*, "Measured viscosity characteristics of $Fe_3O_4$ ferrofluid in magnetic and thermal fields," *Phys. Fluids*, vol. 35, no. 1, p. 012002, Jan. 2023, doi: 10.1063/5.0131551.

[27] M. Anand, "Thermal and dipolar interaction effect on the relaxation in a linear chain of magnetic nanoparticles," *J. Magn. Magn. Mater.*, vol. 522, p. 167538, Mar. 2021, doi: 10.1016/j.jmmm.2020.167538.

[28] X. Liu, Y. Tian, and L. Jiang, "Manipulating Dispersions of Magnetic Nanoparticles," *Nano Lett.*, vol. 21, no. 7, pp. 2699–2708, Apr. 2021, doi: 10.1021/acs.nanolett.0c04757.

[29] C. Kittel, *Introduction to Solid State Physics*. John Wiley & Sons, Inc, 2005.

[30] A. Lavanya, S. Sindhuja, L. Gaurav, and W. Ali, "A Comprehensive Review of Data Visualization Tools: Features, Strengths, and Weaknesses," *Int. J. Comput. Eng. Res. Trends*, vol. 10, no. 1, pp. 10–20, Jan. 2023, doi: 10.22362/ijcert/2023/v10/i01/v10i0102.